

# A Shape-based Reconstruction Technique for DPDW Data

**Misha E. Kilmer**

*Department of Mathematics, Tufts University, Medford MA 02155*  
*mkilme01@tufts.edu*

**Eric L. Miller**

*Department of Electrical and Computer Engineering, Northeastern  
University, Boston, MA, 02115*  
*elmiller@cdsp.neu.edu*

**David Boas**

*NMR Center, Massachusetts General Hospital, Charlestown, MA  
02129*  
*dboas@nmr.mgh.harvard.edu*

**Dana Brooks**

*Department of Electrical and Computer Engineering, Northeastern  
University, Boston, MA, 02115*  
*brooks@cdsp.neu.edu*

**Abstract:** In this paper we give an approach for directly localizing and characterizing the properties of a spatially localized absorption coefficient perturbation as well as coarse scale structure of the background medium from a sparsely sampled, diffuse photon density wavefield. Our technique handles the issues of localization and characterization simultaneously by working directly with the data, unlike traditional techniques which require two stages. To acquire both the structural and quantitative information simultaneously, we model the unknowns as a superposition of a slowly varying perturbation on a background of unknown structure. Our model assumes that the anomaly is delineated from the background by a smooth perimeter which is modeled as a spline curve of unknown knot sequence. The algorithm proceeds by making small perturbations to the curve which are locally optimal. The result is a global, greedy-type optimization approach designed to enforce consistency with the data while requiring the solution to adhere, via regularization, to prior information we have concerning the likely structure of the anomaly. At each step, the algorithm adaptively determines the optimal weighting coefficients describing the characteristics of both the anomaly and the background. The success of our approach is illustrated in two examples provided for a diffuse photon density wave problem arising in a bio-imaging application.

## References and links

1. S. R. Arridge, "Optical tomography in medical imaging," *Inverse Problems*, **15**, R41-R93, (1999).
  2. V. Kolehmainen, S. R. Arridge, W. R. B. Lionheart, M. Vauhkonen, and J. P. Kaipio, "Recovery of region boundaries of piecewise constant coefficients of an elliptic PDE from Boundary Data," *Inverse Problems*, **15**, 1375-1391, (1999).
  3. S. J. Norton and T. Vo-Dinh, "Diffraction tomographic imaging with photon density waves: an explicit solution," *J. Opt. Soc. Am. A*, **15**, 2670-2677 (1998).
  4. M. O'Leary, D. Boas, B. Chance and A. Yodh, "Experimental images of heterogeneous turbid media by frequency domain diffusion photon tomography," *Optics Letters*, **20**, 425-428, (1995).
  5. T. J. Fareel, M. S. Patterson, B. Wilson, "A diffusion theory model of spatially resolved, steady state diffuse reflectance for the non-invasive determination of tissue optical properties *in vivo*," *Med. Phys.*, **19**, 879-888, (1992).
  6. R. C. Haskell, L. O. Svaasand, Tsong-Tseh Tsay, Ti-Chen Feng, Matthew S. McAdams and Bruce J. Tromberg, "Boundary conditions for the diffusion equation in radiative transfer," *J. Opt. Soc. Am. A*, **11**, 2722-2741, (1994).
  7. Per Christian Hansen, "Rank-Deficient and Discrete Ill-Posed Problems," SIAM Press, Philadelphia, 1998.
  8. R. F. Harrington, "Field Computations by Moment Methods," Macmillan, New York, 1968.
  9. M. E. Kilmer, E. L. Miller, D. A. Boas, D. H. Brooks, C. A. DiMarzio and R. J. Gaudette, "Direct object localization and characterization from diffuse photon density wave data," *Proceedings of the SPIE Photonics West Meeting*, Jan. 1999.
- 

## 1 Introduction

In recent years, the problem of forming bio-medical images from sparse observations of diffuse photon density wave data (DPDW) has received considerable attention, [1, 4, 5, 3]. A common goal of such processing is the detection, localization, and characterization of regions in the body, which we refer to as anomalies, that have optical properties (space varying absorption coefficient,  $\mu_a(r)$ , and scattering coefficient,  $\mu_s(r)$ ) that are different from those of the surrounding tissue. By extracting such information about anomalies from the DPDW data, one can potentially draw medically useful conclusions related to the flow of blood in an area, the presence of a tumor, etc.

A typical approach to these problems is the "image-then-detect" method, where the first step is to use measured DPDW data to form an image in two dimensions, or volumetric rendering in 3-D, of a subcutaneous region of interest. This step is followed by image postprocessing via standard techniques to extract and analyze anomalous areas. Thus, the prime difficulty with these methods is the need to first form a pixel by pixel reconstruction of the underlying region, as this step requires the solution to an inverse scattering problem. Since the inverse scattering problem itself is highly ill-posed in the sense that small changes in the data can have dramatic, adverse affects on the estimated solution, no matter which model (Born, Rytov, etc.) is used to approximate the solution to the inverse scattering problem, the computed solution will be hopelessly contaminated by noise artifacts. In order to lessen the sensitivity to noise, some type of regularization technique must be employed. Any number of techniques is possible – our specific choice is described in §3.

A further difficulty with standard approaches is that a small amount of measured DPDW data is used to recover the preliminary image of a large number of pixels. Our approach to the imaging problem is fundamentally different in that we reformulate the problem directly in terms of only a small number of parameters describing the shape, location and contrast of the anomaly as well as the value of the background. As a result, we are able to localize anomalies directly without postprocessing. Our formulation of the problem requires the minimization of a functional with respect to a small number (relative to the total number of pixels reconstructed) of parameters, ensuring the efficiency of the method.

The idea of reducing the number of unknowns by clever parameterization is not new. The authors began to explore this approach for DPDW data in [9]. Another such method that has been applied to DPDW problems is presented in [2]. In that work, the authors use the diffusion equation approximation with piecewise constant diffusion and absorption to model the forward problem. They assume that the finite values of the diffusion and absorption are known a priori, and they seek information about the geometry of the smooth region boundaries where the functions are discontinuous. In other words, they try to solve for the few, unknown parameters that describe the boundaries of each of their curves. Our method is significantly different than the method in [2] for several reasons. We aim to reconstruct maps of the absorption within only two regions, the anomaly and the background. However, we do not need to assume the values of the absorption in different regions a priori: we obtain such information as we simultaneously reconstruct boundaries of the two regions. In the purest form, our model does not restrict the absorption perturbation within the two regions to be constant, although we make that simplification for the results presented here. The method of parameterization of the boundaries in our work and the work in [2] is different. Unlike the method in [2], our method incorporates regularization that helps combat the ill-conditioning and the underdetermined nature of the problem. Finally, the results we present here are for a different geometry than the one used in [2].

The remainder of this paper is organized as follows. In §2, the mathematical model for the diffuse photon density wave system of interest is presented. We describe our algorithm in §3 and provide numerical examples in §4. Finally, we discuss conclusions and future work in §5.

## 2 Models

### 2.1 Forward DPDW Model

In this paper, we consider information extraction algorithms based on the first-Born approximation to the frequency domain, integral equation [9, equation 1] formulation of the diffusion equation describing the flux of the optical modulation envelope. Specifically, for a point source located at position  $r_s$ , the model we have is

$$y(r_k) = -\frac{v}{D} \int_V G(r_k, r') G(r', r_s) g(r') dr' + n(r_k) \quad (1)$$

where  $V$  is the region where the anomaly is assumed to exist (see Fig. 1),  $G(r, r')$  is the Green's function for the problem at hand, and  $g$  represents the space varying perturbation in the absorption coefficient about a known deterministic background used in the specification of  $G$ . The number  $D$  is the diffusion coefficient and  $v$  is the propagation velocity in the medium. Our Green's function is constructed using the extrapolated boundary condition of [6]. We assume that the transmitters can be modeled as point sources on the air-tissue interface. Unlike the work in [9], we consider here a transmission geometry, so the scattered diffuse photon wavefields are measured by an array of  $N_r$  point receivers located below the bottom air-tissue interface (refer to Figure 1).

In this work it is assumed that we have a total of  $N_s$  point sources where the scattered fields generated by each source are observed over an array of  $N_r$  receivers. Thus, for the  $i$ th source, we have a data vector,  $\mathbf{y}_i$ , of length  $2N_r$  comprised of the in-phase and quadrature components of the measured scattered wavefield. Using a method of moments procedure to discretize (1) with pulse basis functions to represent  $g(r)$  [8], we have the discrete equations

$$\mathbf{y}_i = \mathbf{G}_i \mathbf{g} + \mathbf{n}_i, \quad i = 1 \dots, 2N_r, \quad (2)$$

where  $\mathbf{G}_i$  is the discretization of the Born kernel associated with the  $i$ th source,  $\mathbf{g}$  is the vector of pulse basis expansion coefficients for  $g(r)$ , and  $\mathbf{n}_i$  is the noise vector. Finally, all  $\mathbf{y}_i$  are collected into a single vector,  $\mathbf{y}^T = [\mathbf{y}_1^T \dots \mathbf{y}_{N_s}^T]$  to arrive at the discretized data model

$$\mathbf{y} = \mathbf{G}\mathbf{g} + \mathbf{n} \quad (3)$$

with  $\mathbf{G}$  and  $\mathbf{n}$  obtained by “stacking” the  $\mathbf{G}_i$  and  $\mathbf{n}_i$ .

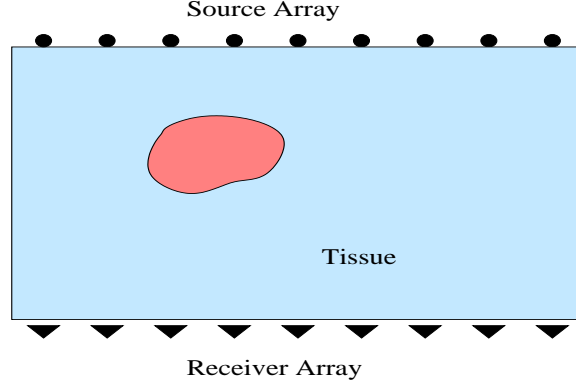


Fig. 1. Source/receiver configuration in the transmission geometry .

## 2.2 A Model for $g(r)$

The model we use here to describe  $g(r)$ , the unknown perturbation in the absorption coefficient, was originally described by the authors in [9]. Here,  $g(r)$  is written as

$$g(r) \equiv S(r)\mathbf{B}_1(r)\mathbf{a}_1 + (1 - S(r))\mathbf{B}_2(r)\mathbf{a}_2, \quad \mathbf{a}_1, \mathbf{a}_2 \in R^{p \times 1}, \quad (4)$$

where  $S(r)$  is an indicator function that is one over the (unknown) support of the object and zero elsewhere. The vectors  $\mathbf{a}_1, \mathbf{a}_2$  hold the expansion coefficients that effectively determine the weight of each function. The  $1 \times p$  vectors  $\mathbf{B}_i$   $i = 1, 2$  have as their components functions  $b_{i,j}(r), j = 1, \dots, p$  which are the expansion functions. In other words, we model the variation of  $g$  over the anomaly as a linear combination of certain functions and the variation of  $g$  on the background as a different linear combination of functions. The particular choice of the  $b_{i,j}$  depends on the application. In this paper, for instance, we assume that there is a homogeneous anomaly of contrast  $a_{1,1}$  against a homogeneous background of value  $a_{2,1}$ : thus,  $\mathbf{B}_1 = b_{1,1}(r) = b_{2,1}(r) = \mathbf{B}_2 = 1$ . In other words, we assume  $g$  is piecewise linear. Use of higher order polynomials, trigonometric functions etc. provides greater flexibility in capturing true, underlying inhomogeneities, but adds a small amount of computational complexity to the problem. In this paper, the objective of the problem is to determine the structure of  $S$  and the  $\mathbf{a}_i$  given a data vector  $y$  related to  $g$  via (1) and assuming the  $\mathbf{B}_i$  are known.

In order to determine the support of the anomaly, and hence the  $S(r)$ , we define the contour of the anomaly as a B-spline curve  $b(s)$ :

$$b(s) = [x(s), y(s)] = \sum_{i=0}^{N-1} B_{k_i}(s)[x_i, y_i], \quad s \in [0, L] \quad (5)$$

for a given set of  $x_i, y_i$  expansion coefficients, or *control points*, and a set of periodic, quadratic,  $B_{k_i}(s)$ . Each  $B_{k_i}(s)$  has support over a subinterval  $[k_i, k_{i+3}] \in [0, L]$ , and the sequence  $\{k_0, \dots, k_{N-1}\}$  is called the *knot* sequence. Since the basis was taken to be

periodic,  $[x_0, y_0] = [x_{N-2}, y_{N-2}]$  and  $[x_1, y_1] = [x_{N-1}, y_{N-1}]$ . According to our model, if  $(x, y)$  is a point outside the curve,  $S(r) = 0$ , otherwise,  $S(r) = 1$ .

From the point of view of discrete implementation of our model,  $\mathbf{S}$  will be a diagonal matrix which functions as the discrete equivalent to  $S(r)$  in (4). If the center of the  $l$ th pixel in the discretization is inside the closed curve  $c(s)$  then we set  $\mathbf{S}_{ll} = 1$ , otherwise we set  $\mathbf{S}_{ll} = 0$ . Define the matrices  $\mathbf{B}_1, \mathbf{B}_2$  to have columns given by  $B_1(x_j, y_i), B_2(x_j, y_i)$  (with  $(x_j, y_i)$  denoting the pixel center coordinates) ordering lexicographically first by increasing  $i$  then by increasing  $j$ . With these definitions the discrete version of (4) is

$$\mathbf{g} = [\mathbf{S}\mathbf{B}_1 \quad (\mathbf{I} - \mathbf{S})\mathbf{B}_2] \begin{bmatrix} \mathbf{a}_1 \\ \mathbf{a}_2 \end{bmatrix} \equiv \mathbf{Q}\mathbf{a} \quad (6)$$

### 3 Algorithm Description

Our algorithm seeks a good approximation to  $g(r)$  by successively improving approximations to  $\mathbf{a}_1, \mathbf{a}_2$ , and  $\mathbf{S}$ . Let  $b^*(s)$  denote the true contour of the true anomaly, and let  $b_0(s)$  denote an initial guess<sup>1</sup> to  $b^*(s)$ . We note that most likely, the number and locations of distinct control points of  $b^*(s)$  and  $b_0(s)$  will be different.

The  $b_0(s)$  defines an initial guess at  $\mathbf{S}$ , which we use to estimate  $\mathbf{a}_1, \mathbf{a}_2$  as the minimizers of

$$J(\mathbf{a}_1, \mathbf{a}_2) := \|\mathbf{G}[\mathbf{S}\mathbf{B}_1, (\mathbf{I} - \mathbf{S})\mathbf{B}_2] \begin{bmatrix} \mathbf{a}_1 \\ \mathbf{a}_2 \end{bmatrix} - \mathbf{y}\|_2. \quad (7)$$

Note that if the number of columns in  $\mathbf{B}_1$  and  $\mathbf{B}_2$  are small (as is the case for problems of interest here) compared to  $2N_s N_r$ , the height of  $\mathbf{G}\mathbf{Q}$ , this problem is quickly and easily solved. The total cost associated with  $b_0(s)$  (hence, with our estimate of the solution  $g_0(r)$ ) therefore is

$$J(\mathbf{a}_1, \mathbf{a}_2) + \lambda \Omega(b_0), \quad (8)$$

where the first term enforces fidelity to the data while the second denotes the regularizer. The regularizer enforces a priori information we have about the shape of the anomaly and serves also to stabilize the least squares solution. In this work, we chose  $\Omega(\mathbf{b})$  to be

$$\Omega(b) = \sum_{i=1}^{K-2} (x_i - x_{i+1})^2 + (y_i - y_{i+1})^2 \quad (9)$$

where  $(x_i, y_i)$  denotes the  $i$ th pair of control points for the current estimate,  $b(s)$ , of  $b^*(s)$ . The idea is that large gaps between adjacent control points are penalized more, thereby discouraging the algorithm from choosing non-physical anomalies. For example, since there are neither sources nor receivers on the sides of the domain we are trying to reconstruct, without regularization we are more likely to reconstruct tall, narrow anomalies in presence of noisy data. Clearly a value of  $\lambda$  that is too large or too small will cause the reconstruction to be under or over dependence on the data, respectively. We do not address the selection of a near optimal parameter here, but refer the interested reader to the abundance of literature on the subject (see [7] and the references therein).

The algorithm proceeds by perturbing the curve  $b_0(s)$  in a fashion to be described shortly to obtain a finite collection of new curves, computing the associated cost (and  $\mathbf{a}_1, \mathbf{a}_2$ ) for each new curve from (8), and then selecting the new estimate,  $b_1(s)$ , of  $b^*(s)$  as a curve which gave the minimum cost over all the perturbations, provided that minimum is less than or equal to the current cost for  $b_0(s)$ . The curves are obtained by

---

<sup>1</sup>An initial guess might be obtained, for example, by taking an image reconstructed by standard techniques, like TSVD, and postprocessing the resulting images to get a rough outline of the anomalous area.

taking each of the  $K - 2$  distinct control points of  $b_0(s)$  and moving them by a fixed amount  $h$  in the vertical, horizontal, and diagonal directions. Thus, there are 8 possible moves for each of the  $K - 2$  distinct control points, resulting in at most  $8(K - 2)$  new curves for which the cost is computed. Then  $b_1(s)$  is selected from among these curves and the process is repeated<sup>2</sup> until the cost can no longer be reduced by making these types of perturbations to the control points of the current estimate  $b_k(s)$ . The algorithm is outlined in Figure 3.

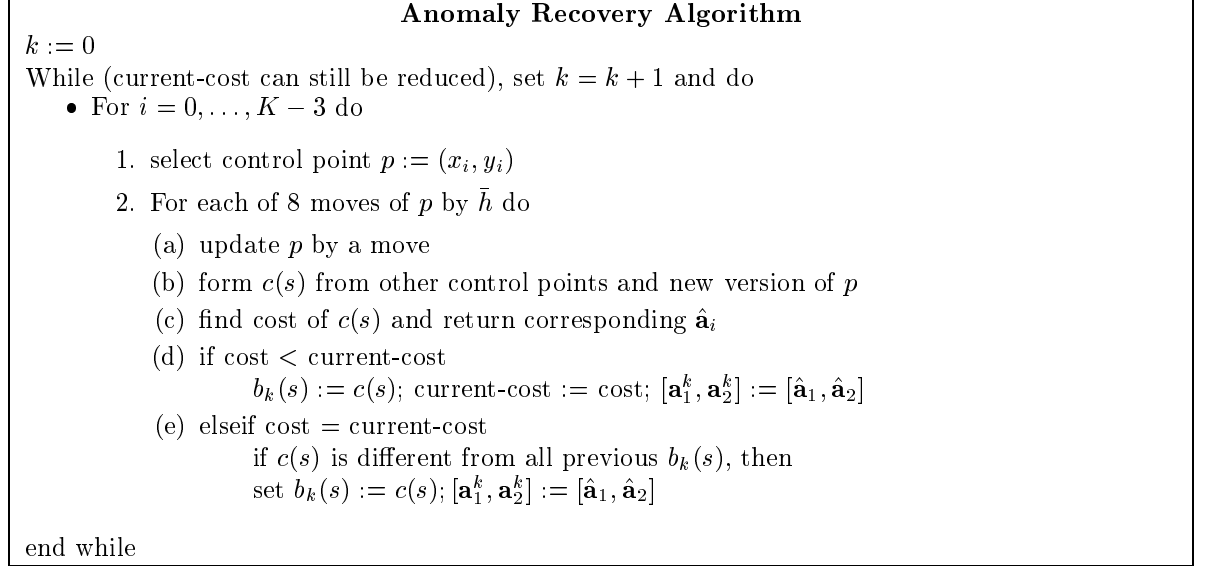


Fig. 2. Anomaly Recovery Algorithm

## 4 Numerical Experiments

All our experiments were conducted in Matlab using double precision, floating point arithmetic. We used Matlab's Spline Toolbox to create and manipulate the b-splines. The region of interest is 3cm in width and 3cm in depth, and the region is discretized into a  $31 \times 31$  pixel image. There were 10 sources across the top of the region and 10 receivers along the bottom. Thus, we created one  $100 \times 31^2$  system matrix  $G$  for each of the 2 modulation frequencies 0 and 200 MHz. The 200 MHz matrix was decomposed into 2 real matrices of the same dimension by treating the in-phase and quadrature components individually. The 3 matrices were then stacked to generate a larger matrix  $\mathbf{G}$ , whose dimensions were  $300 \times 31^2$ .

In both examples, we assumed that the object was a homogeneous perturbation on a homogeneous background of unknown value. Hence, the matrices  $\mathbf{B}_1$  and  $\mathbf{B}_2$  were both taken to be  $m \times 1$  matrices with entries of all ones. Therefore the two coefficients  $\mathbf{a}_1$  and  $\mathbf{a}_2$  were both estimated during the minimization of the cost function in (8). This is different from the work reported in [9] where the  $\mathbf{a}_2$  was taken to be zero both in forming the data and during the reconstruction phase. Recall that  $g(r)$  represents the space varying perturbation in the absorption coefficient,  $\mu_a$ , relative to the the background coefficient used to determine  $\mathbf{G}$ . In our experiments, we used  $\mu_a = .05/\text{cm}$  and  $\mu'_s = 10/\text{cm}$  to construct  $\mathbf{G}$ .

---

<sup>2</sup>perturbations that would take  $b_1(s)$  back to  $b_0(s)$  are disallowed

To generate the data,  $b^*(s)$  was taken to be a quadratic spline curve defined using 6 distinct control points and  $\mathbf{S}^*$  was the corresponding discrete indicator matrix. With  $\mathbf{a}_1^*, \mathbf{a}_2^*$  as the true values of the anomaly and background, respectively, the noise-free data was formed as the matrix-vector product  $\mathbf{G}\mathbf{g}$  with  $\mathbf{g}$  in (6) and  $\mathbf{G}$  described above. This generated a data vector of length 300, the first 100 points of which corresponded to 0 MHz, the second 100 to the in-phase at 200, and the 3rd to the quadrature at 200.

We added shot noise to the data as follows. For a particular source and receiver pair the noise component  $n_{sr}(\omega)$  (at any given frequency  $\omega$ , for either an in-phase or quadrature component) is given by

$$n_{sr}(\omega) = \sigma_{sr}(0)v_1 \quad (10)$$

where  $v_1$  is a number chosen from a normal distribution with mean zero and variance one<sup>3</sup>. Here  $\sigma_{sr}(0)$  is proportional to the total signal strength at DC:

$$\sigma_{sr}(0) = \sqrt{\beta|\tilde{y}_s(r) + \tilde{y}_s^{inc}(r)|} \quad (11)$$

where we denote by  $\tilde{y}_s(r)$  the noise-free scattered field corresponding to source  $s$ , receiver  $r$ , at DC and we use  $\tilde{y}_s^{inc}(r)$  to denote the incident field at source  $s$ , receiver  $r$  at DC. We denote the 300-length, noise-contaminated data vector by  $\mathbf{y}$  and the noise-free data by  $\tilde{\mathbf{y}}$ . The value of the signal to noise ratio that we give in the examples corresponds to

$$SNR = 10 \log_{10} \frac{\|\mathbf{y}\|_2^2}{\|\mathbf{n}\|_2^2}.$$

Since the noise is not white, we must replace  $J(\mathbf{a}_1, \mathbf{a}_2)$  in (7) by

$$J(\mathbf{a}_1, \mathbf{a}_2) := \|\Sigma^{-1} \left( \mathbf{G}[\mathbf{S}\mathbf{B}_1, (\mathbf{I} - \mathbf{S})\mathbf{B}_2] \begin{bmatrix} \mathbf{a}_1 \\ \mathbf{a}_2 \end{bmatrix} - \mathbf{y} \right)\|_{2\cdot},$$

where  $\Sigma^{-1}$  is a diagonal matrix with  $1/\sigma_{sr}(0)$  placed appropriately along the diagonal.

In our examples, we compare the solution computed using our algorithm with the solution obtained via the commonly used truncated singular value decomposition (TSVD) method [7]. Essentially, if  $\mathbf{G} = \sum_{i=1}^n \mu_i \mathbf{u}_i \mathbf{v}_i^T$  is the singular value decomposition of the matrix  $\mathbf{G}$ , the TSVD regularized solution for truncation index  $j, j \leq n$  is  $\mathbf{g}^{tsvd} = \sum_{i=1}^j \frac{\mathbf{u}_i^T \mathbf{y}}{\mu_i} \mathbf{v}_i$ . We refer to the best, or optimal, TSVD solution as the one corresponding to the index  $j$  which gives the smallest relative error in the 2-norm with the true solution.

#### 4.1 Example 1

The contour of the anomaly,  $b^*(r)$ , in this example is the solid green curve in Figure 3 a. We determine our discrete, noise-free data vector  $\tilde{\mathbf{y}}$  by using  $b^*(r)$  to generate  $\mathbf{S}$ , setting  $\mathbf{a}_1 = 17, \mathbf{a}_2 = -1$ , forming  $\mathbf{g}_{true}$  according to (6), and setting  $\tilde{\mathbf{y}} = \mathbf{G}\mathbf{g}_{true}$ . Physically, these values correspond to a background perturbation in  $\mu_a$  from the known value of .05/cm by -.01/cm and a perturbation in  $\mu_a$  within the anomaly of .17/cm. The discretized true image is shown in Figure 3b. We then added a noise vector  $\mathbf{n}$  to the data to generate the noisy data  $\mathbf{y} = \tilde{\mathbf{y}} + \mathbf{n}$ . The noise was determined as described above so that the SNR relative to the data was 20dB.

Figure 3c shows the optimal TSVD solution using the noisy data. Notice that the TSVD reconstruction incorrectly shows the anomaly to be much larger than it should be, and that the computed value of the anomaly is less than 1/5 of what it should be.

<sup>3</sup>We use a different distribution for each of the three data subvectors.

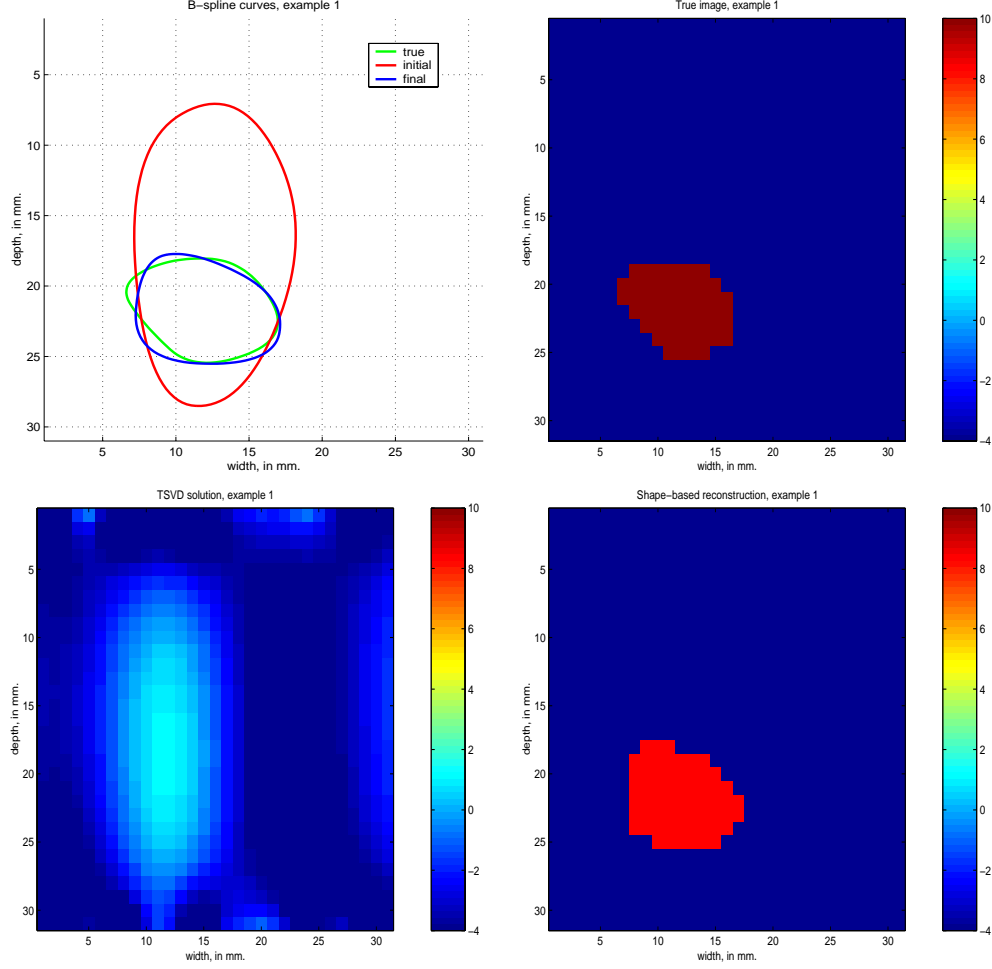


Fig. 3. From left to right, top to bottom: a) Contour curves for  $b^*(r)$ ,  $b_0(r)$ ,  $b_{k^*}(r)$  b) True image of the perturbation in the absorption coefficient c) TSVD reconstruction of the absorption perturbation d) our reconstruction of the absorption using  $h = 1$  and  $\lambda = 6e-9$ .

The relative 2-norm difference error between  $g_{true}$  and  $g_{tsvd}$  (that is, the relative root mean squared error (RMSE)) is  $\|g^{true} - g^{tsvd}\|_2 / \|g^{true}\|_2 = 6.6e-1$ .

Since the TSVD solution was already available, we used this to initialize  $b_0(s)$  for our algorithm. Thus, the red curve in Figure 3a shows  $b_0(s)$  to be an approximation to the outline of where the anomaly appears to be in the TSVD reconstruction, which we obtained by postprocessing the TSVD image manually. We set  $h$ , the amount to perturb the control points, to 1mm in our algorithm and took  $\lambda = 6e-9$  in (9). The final estimate of the contour,  $b_{k^*}(s)$ , that is reached by the algorithm is the blue curve in Figure 3b; that is, no other curve is locally more optimal than that curve. The total reconstruction obtained using our algorithm to determine both  $b_{k^*}(s)$  and  $\mathbf{a}_1, \mathbf{a}_2$  is displayed in Figure 3d. The relative 2-norm error between the true and our computed solution is  $3.2e-1$ , which is a factor of two improvement in the error over the TSVD solution.



## 4.2 Example 2

For our second example, the contour of the anomaly is given by the blue curve in Figure4a. The value of  $g(r)$  inside the anomaly,  $\mathbf{a}_1$  was 20 and the value of the perturbation on the background,  $\mathbf{a}_2$ , was -2. The true solution, illustrated in Figure4b, and noisy data  $\mathbf{y}$  were formed as described in example 1 with the noise computed for a 25 dB SNR.

Figure4c illustrates the TSVD solution. Notice that the value of the anomaly was between 1/4 and 1/3 of what it should have been, and that the anomaly looks to be smeared from top to bottom, as in the first example. This latter phenomenon is to be expected due to the “averaging” nature of the TSVD method and the lack of data at the sides of the region of interest. The relative error between the true solution and TSVD solutions is only 8.6e-1.

Again, because the TSVD solution was available, we manually took an estimate of the outline of the reconstructed anomaly to serve as the initial guess at the contour,  $b_0(s)$ . The curve  $b_0(s)$  is displayed as the red curve in Figure4a. As in the first example, we set the curve perturbation  $h$  to 1mm. For this example, we took  $\lambda = 1\text{e-}7$ .

From the initial estimate, our algorithm took 46 outer iterations until the cost could no longer be reduced any further locally. The final estimate of the contour is shown in blue in Figure4a, while the reconstructed image is displayed in Figure4d. Note the vast improvement of our reconstruction over that obtained by TSVD. We estimate  $\mathbf{a}_1$  as 21.2 and  $\mathbf{a}_2$  as -2. The relative error between the true solution and the estimate obtained by our algorithm was 5.1e-1. Also, the shape of our reconstructed anomaly is only off by 9 pixels with respect to the shape of the true anomaly. Recall from the discussion at the beginning of this section that  $b^*(s)$  was defined with 6 distinct control points while our reconstruction assumed only 5 distinct control points. We believe that if we use more control points for  $b_0(s)$ , we could have reconstructed the irregular contour more accurately. The trade-off for using more control points in the reconstruction is the time it takes to execute one outer iteration.

## 5 Conclusions and Future Work

In this work, we presented an effective technique for simultaneously solving the image formation and object characterization problems from DPDW data with a particular Gaussian noise model. The success of our method was based on the underlying model for the perturbation of the absorption coefficient. Our model formulates the problem in terms of only a small number of unknowns: namely, those that describe the b-spline contour of the anomaly and those that describe the values of the perturbations over both the anomaly and the background. Our examples illustrated that our reconstructions contain significantly more qualitative and quantitative information than the commonly used TSVD reconstructions. Further, although our algorithm was implemented in serial, it is in fact highly parallelizable in that the cost evaluations at any given iteration can be performed in parallel. Thus, it is computationally feasible to consider more complicated structures (i.e. those with more control points that would each need to be perturbed during an iteration). Finally, the model and algorithm presented here are readily adapted to account for non-linear scattering models that arise when the Born approximation is no longer valid. In the future we hope to report results for non-linear scattering models and to generalize this work for scattering problems and 3D reconstructions. The generalization of our approach to multiple anomalies is straightforward if initial estimates of boundaries of such anomalies can be found; more work needs to be done to generalize our method to find multiple anomalies with a single boundary as a starting guess.

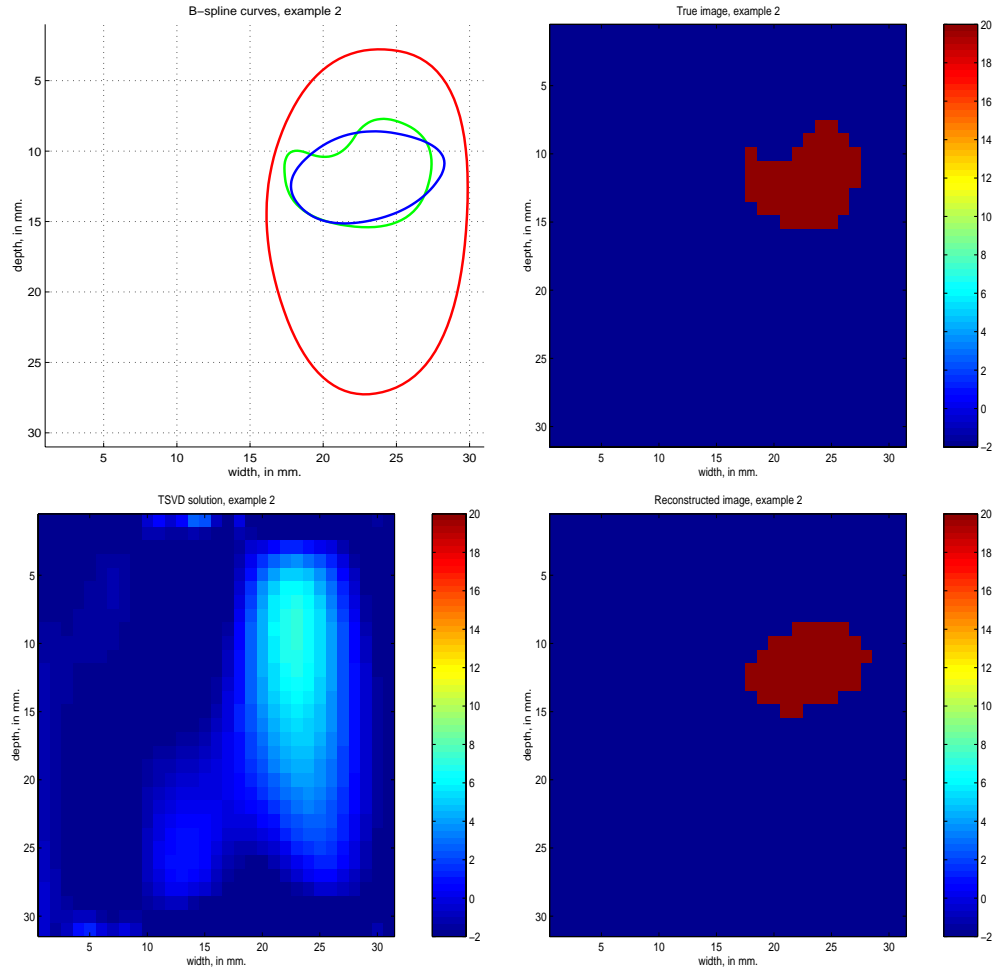


Fig. 4. From left to right, top to bottom: a) Contour curves for  $b^*(r)$ ,  $b_0(r)$ ,  $b_{k^*}(r)$  b) True image of the perturbation in the absorption coefficient c) TSVD reconstruction of the absorption perturbation d) our reconstruction of the absorption using  $h = 1$  and  $\lambda = 1e-7$ .

We note that it is possible to add and delete knots from our description of the contour as well as specify more complicated basis functions  $\mathbf{B}_1$  and  $\mathbf{B}_2$ , thereby allowing reconstruction of more complex anomalies and backgrounds. The question of how to choose  $\lambda$  appropriately is also an important issue. All these considerations were beyond the scope of this work and remain areas for future research.